# Probe measurements in the REPUTE-1 reversed field pinch

H. Ji,[a] H. Toyama, K. Yamagishi, S. Shinohara, A. Fujisawa,[a] and K. Miyamoto
*Department of Physics, Faculty of Science, University of Tokyo, Bunkyo-ku, Tokyo 113, Japan*

(Received 4 June 1991; accepted for publication 23 June 1991)

A four-channel triple-probe and magnetic-probe array, a complex probe which consists of three types of probes and two eight-channel magnetic-probe (poloidal and toroidal) arrays, has been installed in the revised field pinch University of Tokyo experiment (REPUTE-1) reversed field pinch (RFP) device. Mean and fluctuation parts of plasma parameters, including the three components of magnetic fields, three components of electric fields, electron density, electron temperature, and space potential, are measured in $0.5a \lesssim r \leqslant a$ region. The triple-probe method and the electric field measurement are described in detail, and effects due to the fast electrons, etc., are discussed. Some experimental examples obtained in the REPUTE-1 RFP plasma are given, and the detailed results will be published elsewhere.

## I. INTRODUCTION

Recently, it has been experimentally clarified that behavior of edge plasma is closely related with global confinement characteristics, especially in some important operating modes, such as the *H*-mode in tokamaks. Interactions between plasma and wall surface are also determined by the behavior of the edge plasma.[1] For the purpose of understanding edge plasma, it is important to have experimental information on the basic plasma parameters including electron density $n$, electron temperature $T_e$, etc. Information on fluctuations, such as fluctuation levels and correlations between fluctuations, are also important as well as the mean values, as anomalous transport is generally attributed to the fluctuations.[2] Conventionally, probe methods[3–6] have been intensively used in edge diagnostics because of their good spatial resolutions and conveniences, although they are limited in use only at the relatively cold region. In order to measure the mean and fluctuation parts of plasma parameters, various types of Langmuir probes and magnetic probes have been designed and installed in the reversed field pinch university of Tokyo experiment REPUTE-1[7] reversed field pinch (RFP). Especially, the triple-probe method has been developed to meet the request of measuring density and temperature fluctuations simultaneously in a turbulent plasma. In this paper, we give a description of our measurements via Langmuir probes and magnetic probes including their measuring principles and hardwares, and detailed experimental results will appear elsewhere.

First, measurement principles are described in Sec. II. After a brief summary about Langmuir probe measurements, the triple-probe method and the electric field measurement are described and discussed in detail. In Sec. III, we present the hardware structures of various probes, including a triple-probe and magnetic-probe array, a complex probe which consists of three different types of probes (triple-probe, double-probe, and magnetic-probe), a poloidal and a toroidal array of magnetic probes. Also, a probe drive circuit and data-acquisition electronics are described in the same section. Some examples of our probe measurements will be given in the final section (Sec. IV).

[a]Present address: National Institute for Fusion Science, Nagoya 464-01, Japan.

## II. MEASUREMENT PRINCIPLES

### A. Characteristic of Langmuir probe without magnetic field

There have been many treatments of the plasma-sheath problem published with respect to electric probes inserted into the plasma since Tonks and Langmuir.[8] Unfortunately, no complete and rigorous theory exists to cover the many regimes in which a Langmuir probe can be used. Nevertheless, there are a number of well established approximate formulas which are used practically in the experiments. In the following, we briefly summarize the probe characteristics in collisionless plasma without magnetic field firstly.

When the probe potential is higher than the space potential, i.e., $V > V_s$, the probe current is limited by the electron saturation current:

$$I_- = \tfrac{1}{4} enA_- \sqrt{8\,T_e/\pi m_e}, \tag{1}$$

where $T_e$ is electron temperature in eV unit, $n$ is the electron density, $A_-$ is the electron collection area. Decreasing the probe potential, $V < V_s$, the electron current is modified by the Boltzmann factor $\exp[(V - V_s)/T_e]$. When the electron current is reduced to be equal to the ion current, the total current will become zero, then $V = V_f$ (floating potential). Decreasing the bias potential further, only ions are eventually collected, and probe current reaches the ion saturation current $I_+$. In order to form a stable sheath, Bohm showed that there must exist a presheath region between the sheath and plasma.[9] In the case of ion temperature $T_i = 0$ in the plasma region, the ions are accelerated to the ion acoustic speed $C_s = \sqrt{T_e/m_i}$ toward the probe in order to provide the ion collection current. The ion saturation current $I_+$ is given approximately as follows:[6]

$$I_+ = \exp(-1/2) A_+ enC_s. \tag{2}$$

[Note that $\exp(-1/2) \simeq 0.61$]. Here $A_+$ is the ion collection area. If finite ion temperature in the plasma region is

 0034-6748/91/102326-12$02.00  

considered, the problem is much more complicated and ion orbits in specified geometry must be analyzed. Exact numerical solutions for arbitrary $T_i/T_e$ and sheath thickness have been calculated by Laframboise,[10] providing the ion and electron currents. His results showed that the dependence of $I_+$ upon ion temperature is weak if $T_i < T_e$ when the sheath is much thinner than the probe size. For the cases of $T_i \sim T_e$ or $T_i > T_e$ as in the REPUTE-1 RFP, unfortunately there is no generally accepted theory to predict the ion collection current exactly. However, an approximate formula which is used practically in experiments is given by $C_s = \sqrt{(T_e + T_i)/m_i}$ in Eq. (2).[11] We use this formula to calculate density $n$ from given values of $A_+$, $I_+$, and $T_e$ assuming a value of $T_i$. The Langmuir probe characteristics in the collisionless plasma without magnetic field can be summarized as follows:

$$I = \begin{cases} -I_- \exp\left(\dfrac{V - V_s}{T_e}\right) + I_+, & V < V_s; \\ -I_-, & V \geqslant V_s. \end{cases} \tag{3}$$

When $I=0$, the floating potential $V_f$ is given by

$$\frac{V_f - V_s}{T_e} = -\ln\left(\frac{A_-}{A_+}\sqrt{\frac{em_i}{2\pi m_e(1 + T_i/T_e)}}\right). \tag{4}$$

When the mean free path is smaller than the probe size, the collisions can reduce the collection current. However, since the mean free path ($\geqslant$ a few cm) is much larger than the probe size ($\leqslant$1 mm) in the REPUTE-1 edge plasma, we do not need to consider the collisional effects.

### B. Effects of magnetic fields

The importance of the magnetic field effects is dependent on the ratio of Larmor radius $\rho$ to the typical dimension $a_p$ of the probe. Because the electron Larmor radius $\rho_e$ is smaller than the ion radius $\rho_i$ (for the case of comparable $T_e$ and $T_i$ values) by the factor $\sqrt{m_e/m_i}$, the electrons are more strongly affected than the ions. We can classify the magnetic fields into three regions: a weak field in which $\rho_{i,e} \gg a_p$, a strong field in which $\rho_i \gg a_p \gg \rho_e$, and a very strong field in which $a_p \gg \rho_{i,e}$. Clearly, in the weak fields, the probe characteristics described above can be used without any modifications.

In the strong fields, the ion collection is unaffected, while the electron saturation current is decreased due to the fact that the effective electron collection area $A_-$ is not the total probe surface but the projection of the surface in the direction of the fields. The electron collection along the flux tube is balanced by a cross field diffusion due to both classical and anomalous processes.[12] This problem is equivalent to the anomalous transport problem, therefore, it is still unsolved. Fortunately, if the probe is sufficiently negative to the space potential so that most of electrons are reflected, such as when the probe is operated around the floating potential, then electron collection current is still governed by the thermal Boltzmann factor as before.[6]

In the very strong fields $a_p \gg \rho_{i,e}$, the situation becomes more complicated, because the ion collection along the flux tube is balanced by a cross field diffusion again, like electron collection. Recently, in connection with analyses of the plasma flows in the scrape-off region (between the main plasma and wall), several approaches have been performed using a fluid theory[11,13–18] and kinetic treatment[19–23] (since the analysis of Harrison and Thompson[24]). Notwithstanding, no simple analytic expression for probe characteristics has been obtained, and the problem remains an open question. Accordingly, it is better to avoid this situation in the practical experiments, i.e., let the probe size $a$, sufficiently smaller than $\rho_i$.

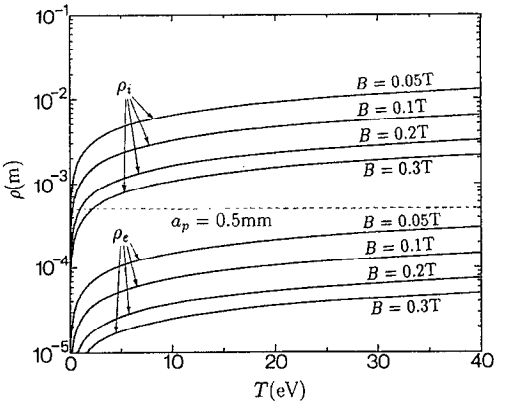


FIG. 1. Electron and ion Larmor radius $\rho_{e,i}$ vs temperature for several magnetic fields $B$.

Figure 1 shows the dependence of Larmor radius $\rho_e$, $\rho_i$ on the temperature $T_{e,i}$, at several strengths of magnetic field. In the low current discharge ($I_p \sim 100$ kA) in REPUTE-1, the values of $B$ and $T_{e,i}$ are $B \sim 0.1$ T and $T_e \sim T_i \leqslant 20$ eV in the edge region, respectively. The value of $a_p$ is designed to be 0.5 mm, in order to satisfy the condition $\rho_i \gg a_p \gg \rho_e$. Therefore, if we bias the probes around $V_f$, the probe characteristic Eq. (3) can be used with only one modification in electron collection area, i.e., using the projection area in the direction of $B$ instead of total probe area.

### C. Triple-probe measurement

The main disadvantage of single or double probe is that they require the voltage sweep to obtain the probe characteristic curves. This requirement limits the time resolution of measurement and makes them difficult to be used in time-varying plasma. A method of using the triple-probe has been proposed to overcome this disadvantage.[25] Another similar method has been also used in the Poloidal Divertor Experiment (PDX) tokamak.[4] An additional (fourth) probe tip used to reduce the effect of nonuniform space potential is described in the second subsection. The effects of fast electrons on the measurements are discussed in the third subsection.

#### *1. Description of the method*

Let us consider that three probes $P_1$, $P_2$, and $P_3$ are inserted into the plasma, as shown in Fig. 2(a). A constant voltage $V_{d3}$ is applied between $P_1$ and $P_3$, and the probe current is $I_1$. Let $V_{d2}$ denote the potential difference between $P_1$ and floating $P_2$. If we assume that the space po-

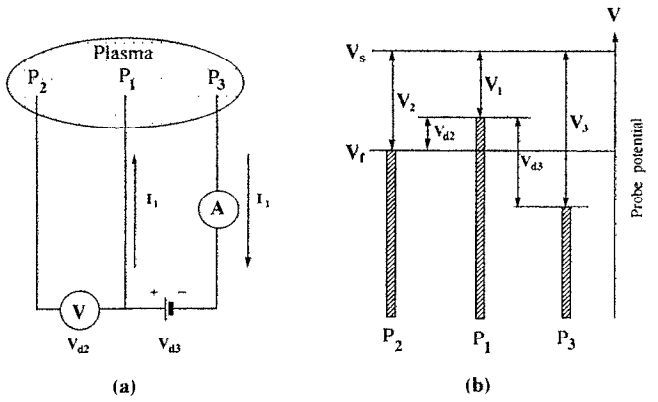


FIG. 2. (a) Triple-probe circuit, and (b) potential of each probe.

tential $V_s$ is uniform in the region of the probes and let $V_1$, $V_2(\equiv V_s - V_f)$, and $V_3$ express the potential difference of probes from $V_s$, as shown in Fig. 2(b), then we have

$$V_{d2}=V_2-V_1, \tag{5}$$

$$V_{d3}=V_3-V_1. \tag{6}$$

Next, with the use of Eq. (3), the currents flowing into the three probes may be written as

$$-I_1=-I_-\exp\left(-\frac{V_1}{T_e}\right)+I_+, \tag{7}$$

$$0=-I_-\exp\left(-\frac{V_2}{T_e}\right)+I_+, \tag{8}$$

$$I_1=-I_-\exp\left(-\frac{V_3}{T_e}\right)+I_+. \tag{9}$$

Combined with Eqs. (5) and (6), Eqs. (7)–(9) are solved with respect to $T_e$ and $I_+$:

$$\frac{1}{2}=\frac{1-\exp(-V_{d2}/T_e)}{1-\exp(-V_{d3}/T_e)}, \tag{10}$$

$$I_+=I_1\frac{\exp(-V_{d2}/T_e)}{1-\exp(-V_{d2}/T_e)}. \tag{11}$$

If the probe currents and voltages are monitored, the electron temperature $T_e$ can be reduced by Eq. (10), and the approximate value of electron density $n$ can be obtained with the use of Eqs. (11) and Eq. (2) assuming a value of $T_i$. The time resolutions of $T_e$ and $n$ measurements are only limited by the data sampling.

Figure 3(a) shows the relations between the electron temperature $T_e$ and the measured voltage $V_{d2}$ for various applied voltage $V_{d3}$ from 15 to 40 V. The dependences of ion saturation current $I_+$ (or equivalently $n$) upon $V_{d2}$ are also shown in Fig. 3(b). It can be seen that curves have a good linearity in the region $T_e < V_{d3}/2$, and divergent when $T_e > V_{d3}/2$. In the limit of $T_e \ll V_{d3}$, Eq. (10) becomes

$$\frac{T_e}{V_{d2}}\simeq\frac{1}{\ln 2}\simeq 1.44. \tag{12}$$

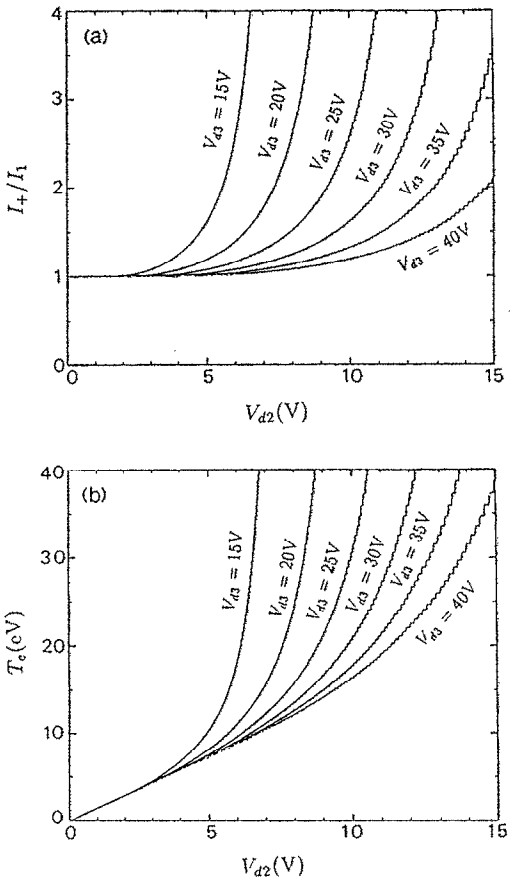


FIG. 3. Dependences of the electron temperature $T_e$ (a) and ion saturation current $I_+$ (b) upon the measured voltage $V_{d2}$ for various applied voltage $V_{d3}$.

We conclude that the accurate measurement of $T_e$ requires the applied voltage of $V_{d3} \geqslant 2T_e$.

### 2. Effect of nonuniform space potential

In the above arguments, it is assumed that the space potential $V_s$ or $\phi$ is uniform between the probes. If there exist differences of $V_s$ between probes, i.e., there exists an electric field parallel to the probe tips, it is necessary to correct this effect. The $V_f$ fluctuation power spectra as a function of wavenumber in REPUTE-1 have been measured by two Langmuir probes fixed in space.[26] It has been found that the typical wavenumber of the potential fluctuations is $\lesssim 0.5\ \mathrm{cm}^{-1}$, i.e., the wavelength is $\gtrsim 12$ cm, which is much larger than probe separation 0.3 cm in our measurements. Therefore, the correction of $V_{d2}$ can be measured using $P_1$ and an additional probe $P_4$ lying in the same direction of $P_1$ and $P_2$. Figure 4 shows the triple-probe circuit with the additional probe $P_4$. The influence of parallel electric field can be ruled out simply by

$$V_{d2}=(V_{d2}^1+V_{d2}^2)/2, \tag{13}$$

as can be tested as following.

We assume that the electrostatic potential fluctuation has a form of

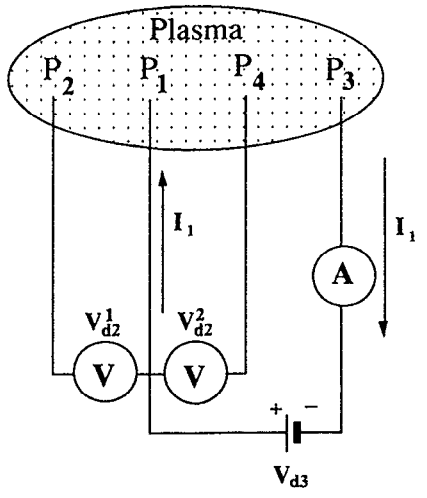


FIG. 4. Triple-probe circuit with an additional probe.

$$\tilde{\phi}(x)=\phi_0 \sin(\bar{k}x+\alpha), \tag{14}$$

where $\phi_0$ is the amplitude of the potential fluctuation, $\bar{k}$ is a typical (or the averaged) wavelength, and $\alpha$ is a random phase. Let $x_1$, $x_2$, and $x_3$ be the locations of $P_2$, $P_1$, and $P_4$, respectively; the probe separation $\Delta x$ is $\Delta x = x_2 - x_1 = x_3 - x_2$. We have

$$V_{d2}^1 = V_{d2} + \tilde{\phi}(x_2) - \tilde{\phi}(x_1), \tag{15}$$

$$V_{d2}^2 = V_{d2} + \tilde{\phi}(x_2) - \tilde{\phi}(x_3), \tag{16}$$

therefore,

$$\begin{aligned} V_{d2} - (V_{d2}^1 + V_{d2}^2)/2 &= \tfrac{1}{2}\{[\tilde{\phi}(x_2) - \tilde{\phi}(x_1)] + [\tilde{\phi}(x_2) - \tilde{\phi}(x_3)]\} \\ &= 2\phi_0 \sin(\bar{k}x_2 + \alpha)\sin^2(\tfrac{1}{2}\bar{k}\Delta x). \end{aligned} \tag{17}$$

The relative difference becomes

$$\left|\frac{V_{d2} - (V_{d2}^1 + V_{d2}^2)/2}{V_{d2}}\right| \leqslant 2\frac{\phi_0}{V_{d2}}\left(\frac{1}{2}\bar{k}\Delta x\right)^2, \tag{18}$$

where

$$\frac{\phi_0}{V_{d2}} = \frac{\sqrt{2}|\tilde{\phi}|}{T_e}\frac{T_e}{V_{d2}} \cong 2.0. \tag{19}$$

$[|\tilde{\phi}|/T_e \sim 1$ (Ref. 27)]. From $(1/2)\bar{k}\Delta x \sim 0.08$, the right-hand side of Eq. (18) becomes 2.5%. Effect of the nonuniform space potential on $V_{d3}$ is smaller because of the larger value of $V_{d3}$. As a result, with the use of the additional probe tip, nonuniform space potential between the probe tips introduces ambiguities of only $\sim$2.5% and $\sim$6% in $T_e$ and $n$ measurements.

### 3. Effect of fast electrons

Recent experiments showed that fast electrons exist in the ZT-40M RFP edge ($r \sim a$) region.[28] These fast electrons also have an effect on the interpretation of probe data, as will be discussed below.

We denote the density and temperature of fast electrons by $n^F$ and $T_e^F$, respectively, and assume $n^F/n = \alpha \ll 1$ and $T_e^F/T_e = \beta > 1$. Secondary electrons due to the fast electrons will also affect the measurements. Usually, emission coefficient of the secondary electrons is a function of incident energy. For simplicity, we introduce the energy averaged coefficient $\gamma$ as in the Ref. 28. Then Eqs. (7)–(9) are modified to

$$-I_1 = -I_- \exp\left(-\frac{V_1}{T_e}\right) - \alpha\sqrt{\beta}(1-\gamma)I_- \exp\left(-\frac{V_1}{\beta T_e}\right) + I_+, \tag{20}$$

$$0 = -I_- \exp\left(-\frac{V_2}{T_e}\right) - \alpha\sqrt{\beta}(1-\gamma)I_- \exp\left(-\frac{V_2}{\beta T_e}\right) + I_+, \tag{21}$$

$$I_1 = -I_- \exp\left(-\frac{V_3}{T_e}\right) - \alpha\sqrt{\beta}(1-\gamma)I_- \exp\left(-\frac{V_3}{\beta T_e}\right) + I_+, \tag{22}$$

where $I_+$ is assumed not to be strongly affected by the fast electrons. We define

$$\eta = \frac{I_-}{I_+} = \frac{A_-}{A_+}\sqrt{\frac{em_i}{2\pi m_e(1+T_i/T_e)}}, \tag{23}$$

and $\eta \simeq 8.3$ assuming $T_i/T_e \simeq 2$ in our case. Therefore, Eq. (21) becomes

$$\eta Z^\beta + \alpha\sqrt{\beta}(1-\gamma)\eta Z = 1, \tag{24}$$

where $Z = \exp(-V_2/\beta T_e)$. Since $V_2 \equiv V_s - V_f$, if $\alpha$, $\beta$, and $\gamma$ are given, $Z$ then $(V_f - V_s)/T_e$ can be determined by solving Eq. (24). Instead of Eqs. (10) and (11), we have

$$\frac{1}{2} = \frac{1-\exp(-V_{d2}/T_e) + \alpha\sqrt{\beta}(1-\gamma)[1-\exp(-V_{d2}/\beta T_e)]\exp[-(\beta-1)/\beta(V_{d2}/T_e)]/Z^{\beta-1}}{1-\exp(-V_{d3}/T_e) + \alpha\sqrt{\beta}(1-\gamma)[1-\exp(-V_{d3}/\beta T_e)]\exp[-(\beta-1)/\beta(V_{d3}/T_e)]/Z^{\beta-1}}, \tag{25}$$

$$I_+ = I_1 \frac{\exp(-V_{d2}/T_e)}{1-\exp(-V_{d3}/T_e) - \alpha\sqrt{\beta}(1-\gamma)\eta Z\{1-\exp[-(\beta-1)/\beta(V_{d2}/T_e)]\}}. \tag{26}$$

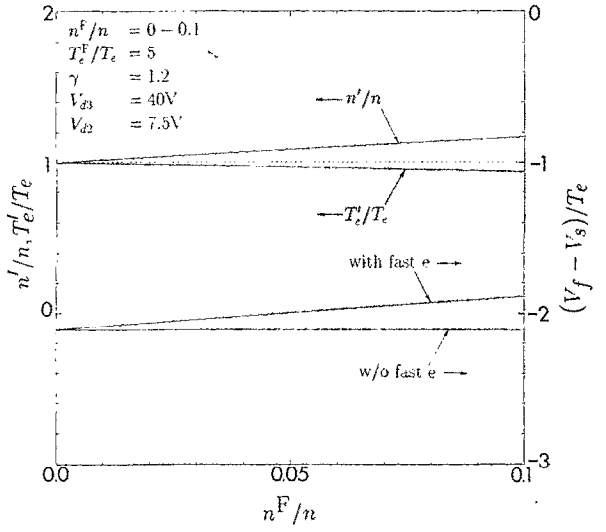


FIG. 5. $\alpha \equiv n^F/n$ dependence of $T_e'/T_e$, $n'/n$, and $(V_f - V_s)/T_e$. Here, $T_e'$ and $n'$ are electron temperature and density determined by ignoring the effects of fast electrons (let $\alpha = 0$).

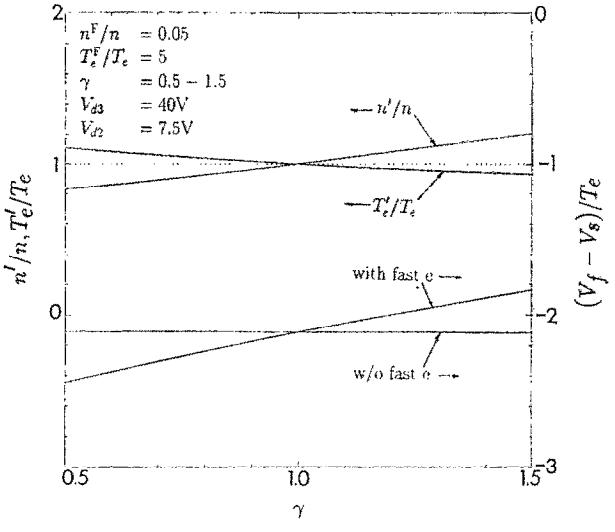


FIG. 7. Secondary electron emission coefficient $\gamma$ dependence of $T_e'/T_e$, $n'/n$, and $(V_f - V_s)/T_e$. Here, $T_e'$ and $n'$ are electron temperature and density determined by ignoring the effects of fast electrons (let $\alpha = 0$).

In Figs. 5–7, the dependences of $T_e'/T_e$, $n'/n$, and $(V_f - V_s)/T_e$ on the parameters $\alpha$, $\beta$, and $\gamma$ are shown. Here, $T_e'$ and $n'$ are electron temperature and density determined by ignoring the effects of fast electrons (let $\alpha = 0$). It can be seen that the fast electrons do not affect the measurements via triple-probe seriously, if $\alpha$ is sufficiently smaller than unit. For example, in the case of $\alpha = 5\%$, $\beta = 5$, and $\gamma = 1.2$ as in the ZT-40M edge,[28] $T_e$ is underestimated by $\sim 3\%$ while $n$ is overestimated by $\sim 8\%$. Including the effect from nonuniform space potential discussed previously, we conclude that $T_e$ and $n$ are determined using our triple probes with accuracies of $\lesssim 5\%$ and $\lesssim 15\%$, respectively.

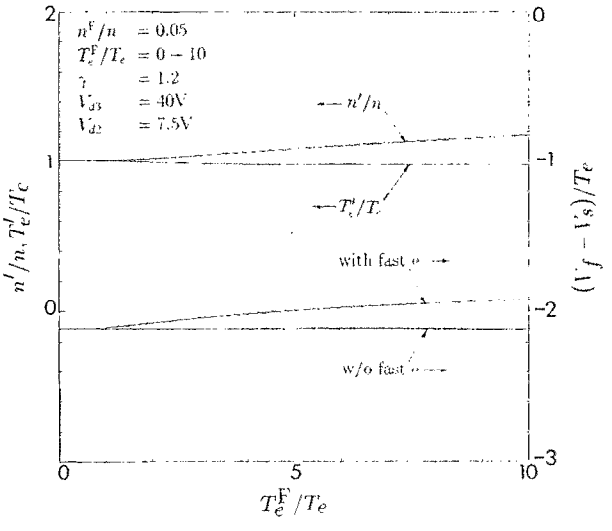


FIG. 6. $\beta \equiv T_e^F/T_e$ dependence of $T_e'/T_e$, $n'/n$, and $(V_f - V_s)/T_e$. Here, $T_e'$ and $n'$ are electron temperature and density determined by ignoring the effects of fast electrons (let $\alpha = 0$).

## D. Measurement of electric field fluctuation

### 1. Description of the method

Let us consider measurement of the electric field fluctuation using a floating double probe. If the wavelength of electrostatic potential fluctuation is much longer than the probe separation and a difference of the electron temperature between the probes is negligible, the electrostatic field can be approximately obtained by dividing difference in the floating potential by the probe separation. This can be simply tested in the model of Eq. (14) again. The electrostatic field fluctuation $\tilde{E}_x$ becomes

$$\tilde{E}_x(x) = -\frac{\partial \tilde{\phi}(x)}{\partial x} = -\bar{k}\phi_0 \cos(\bar{k}x + \alpha). \tag{27}$$

On the other hand, from the potential measurements at the two points $x_1$ and $x_2$, we have

$$\tilde{E}_x' = -\frac{\tilde{\phi}(x_2) - \tilde{\phi}(x_1)}{x_2 - x_1}$$

$$= -\bar{k}\phi_0 \cos\left(\bar{k}\frac{x_1 + x_2}{2} + \alpha\right)\frac{\sin\left(\frac{1}{2}\bar{k}\Delta x\right)}{\frac{1}{2}\bar{k}\Delta x}, \tag{28}$$

where $\Delta x = x_2 - x_1$. In the limit of $\frac{1}{2}\bar{k}\Delta x \ll 1$, $\tilde{E}_x'$ becomes

$$\tilde{E}_x' = \tilde{E}_x\left(\frac{x_1 + x_2}{2}\right)\left[1 - \frac{1}{6}\left(\frac{1}{2}\bar{k}\Delta x\right)^2 + \ldots\right]. \tag{29}$$

In our case of $\bar{k} \sim 0.5\ \mathrm{cm}^{-1}$ (Ref. 26) and $\Delta x = 0.3$ cm, the value of $\frac{1}{2}\bar{k}\Delta x$ becomes $\sim 0.08 \ll 1$. Therefore, $\tilde{E}_x'$ gives a good approximation of $\tilde{E}_x$ within an error of 0.1%.

### 2. Effect of electron temperature fluctuation

If there exists the large electron temperature fluctuation $\tilde{T}_e$, $\tilde{E}(\equiv -\nabla\tilde{V}_f)$ measured by the double probe is then different from $\tilde{E}^*(\equiv -\nabla\tilde{V}_s)$ in the relation of

$$\tilde{E}=\tilde{E}^*+c\nabla\tilde{T}_e, \tag{30}$$

where $c$ is a constant defined by the right-hand side of Eq. (4) ($c\simeq 2.1$ in our case). In this case $\tilde{E}$ does not give the direct measurement of $\tilde{E}^*$, instead, some information on the correlations and amplitude can be obtained under certain conditions.

The measured fluctuations usually have linear dispersion relations[29–31] so that they can be expressed as a sum of plane waves with a constant phase velocity. In this case, a correlation between $\tilde{\alpha}$ and $\tilde{\beta}$ defined by

$$\langle\tilde{\alpha}\tilde{\beta}\rangle\equiv\lim_{T\to\infty}\frac{1}{T}\int_{-T/2}^{T/2}\tilde{\alpha}(x,t)\tilde{\beta}(x,t)dt|_{x=x_0} \tag{31}$$

can be rewritten to the form of

$$\langle\tilde{\alpha}\tilde{\beta}\rangle=\lim_{X\to\infty}\frac{1}{X}\int_{-X/2}^{X/2}\tilde{\alpha}(x,t)\tilde{\beta}(x,t)dx|_{t=t_0} \tag{32}$$

in the steady state, where $x$ is the toroidal/poloidal coordinate and $t$ is the time. We multiply Eq. (30) by $\tilde{T}_e$ and take its correlation with the use of Eq. (32). Since the last term

$$(c/2)\lim_{X\to\infty}\frac{1}{X}[\tilde{T}_e^2]_{x=-X/2}^{x=X/2}$$

is zero, we obtain

$$\langle\tilde{T}_e\tilde{E}\rangle=\langle\tilde{T}_e\tilde{E}^*\rangle. \tag{33}$$

Next we multiply Eq. (30) by $\tilde{n}$ and take its correlation:

$$\langle\tilde{n}\tilde{E}\rangle=\langle\tilde{n}\tilde{E}^*\rangle+\sum_k k\tilde{T}_e(k)\tilde{n}(k)\sin\theta_{n,T_e}(k), \tag{34}$$

where $\tilde{T}_e(k)$ $[\tilde{n}(k)]$ is the Fourier amplitude of $\tilde{T}_e(x)$ $[\tilde{n}(x)]$ for wavenumber $k$, and $\theta_{n,T_e}(k)$ is the phase difference. If $\sin\theta_{n,T_e}(k)\simeq 0$, i.e., $\tilde{n}$ is in phase or antiphase with $\tilde{T}_e$, the last term in Eq. (34) becomes negligible then $\langle\tilde{n}\tilde{E}\rangle$ gives the measurement of $\langle\tilde{n}\tilde{E}^*\rangle$. If $\sin\theta_{n,T_e}(k)\neq 0$, the wavenumber spectra of $\tilde{T}_e$ and $\tilde{n}$ must be measured simultaneously.

We multiply Eq. (30) by $\tilde{E}$ and $\tilde{E}^*$, and obtain the following equations in the same way:

$$|\tilde{E}|^2=\langle\tilde{E}\tilde{E}^*\rangle+\sum_k k\tilde{T}_e(k)\tilde{E}(k)\sin\theta_{T_eE}(k), \tag{35}$$

$$\langle\tilde{E}\tilde{E}^*\rangle=|\tilde{E}^*|^2+\sum_k k\tilde{E}^*(k)\tilde{E}(k)\sin\theta_{E^*,E}(k). \tag{36}$$

If $\sin\theta_{T_eE}\simeq 0$, then we have $\sin\theta_{E^*,E}\simeq 0$ due to Eq. (33), hence the relation of $|\tilde{E}|^2\simeq\langle\tilde{E}\tilde{E}^*\rangle\simeq|\tilde{E}^*|^2$ can be derived from Eqs. (35) and (36).

As a summary, even in the case of the large $\tilde{T}_e$ (i.e., $c|\tilde{T}_e|\sim|\tilde{V}_s|$), with the use of $\tilde{E}$ measured by a floating double probe, $\langle\tilde{T}_e\tilde{E}^*\rangle$ can be always obtained. On the other hand, $\langle\tilde{n}\tilde{E}^*\rangle$ and $|\tilde{E}^*|$ can be also obtained if the fluctuations $\tilde{n}$, $\tilde{T}_e$, and $\tilde{E}$ are in phase or antiphase with each other. Otherwise, the wavenumber spectra of the fluctuations or $\tilde{E}^*$ must be directly measured.

### 3. Effect of fast electrons

If there exist the fast electrons, some modifications must be applied in Eq. (30). In the limit of $n^F/n\ll 1$, from Eq. (21) we have

$$V_s-V_f=cT_e+\frac{n^F}{n}\sqrt{\frac{T_e^F}{T_e}}(1-\gamma)\eta^{1-T_e/T_e^F}T_e. \tag{37}$$

By introducing the fluctuating parts into Eq. (37) (e.g., replacing $n^F$ by $n^F+\tilde{n}^F$) and taking its first order, we derive

$$\tilde{V}_s-\tilde{V}_f=c\tilde{T}_e+\alpha\sqrt{\beta}(1-\gamma)\eta^{1-1/\beta}\left[\frac{\tilde{n}^F}{n^F}-\frac{\tilde{n}}{n}+\left(\frac{1}{2}+\frac{c}{\beta}\right)\frac{\tilde{T}_e^F}{T_e^F}\right]T_e. \tag{38}$$

In the case of $n^F/n=5\%$, $T_e^F/T_e=5$ and $\gamma=1.2$, the above equation becomes

$$\tilde{V}_s-\tilde{V}_f=c\tilde{T}_e+\left[c'\left(\frac{\tilde{n}^F}{n^F}-\frac{\tilde{n}}{n}\right)+c''\frac{\tilde{T}_e^F}{T_e^F}\right]T_e, \tag{39}$$

where $c\simeq 2.1$, $c'\simeq -0.12$, and $c''\simeq -0.11$. The last term in Eq. (39) is estimated to be $\lesssim 20\%$ of $c\tilde{T}_e$ assuming $\tilde{n}^F/n=\tilde{n}^F/n^F\lesssim 0.4$ and $\tilde{T}_e/T_e=\tilde{T}_e^F/T_e^F\lesssim 0.3$. Therefore, the effect of the fast electrons is considerably smaller than that due to $\tilde{T}_e$ in the usual electric field measurements.

## III. HARDWARE

### A. Triple-probe and magnetic-probe array

The structure of the probe array is shown in Fig. 8. It has four channels, each of them consists of five electric tips and a three-component magnetic probe. The separation between the neighboring channels is 15 mm.

In one channel, four tips are used as a triple-probe (the reason for the use of fourth tip has been explained in Sec. I C) measuring the plasma density $n$ and temperature $T_e$, and one remaining tip is used as a single-probe measuring floating potential $V_f$. The distances between tips are 3 or 5 mm. Each electric tip has a diameter of 0.5 mm with an exposed length of 0.5 mm. The feedthrough wire is connected to the electric probe by a fix screw having a diameter of 1.2 mm.

The electric tips are made of Molybdenum which has a high melting point and large specific heat so it can withstand high heat fluxes. The probe array house is made of glass ceramic which can withstand the high heat fluxes and have a flexibility allowing complex processes. The Molybdenum tips are fixed between two ceramic plates of 3 mm in thickness. The leads from the Langmuir probes are transmitted to a probe driver in a shielded box including the power supplies and isolation amplifies.

A three-components magnetic-probe array is also installed inside the probe array house, in order to measure

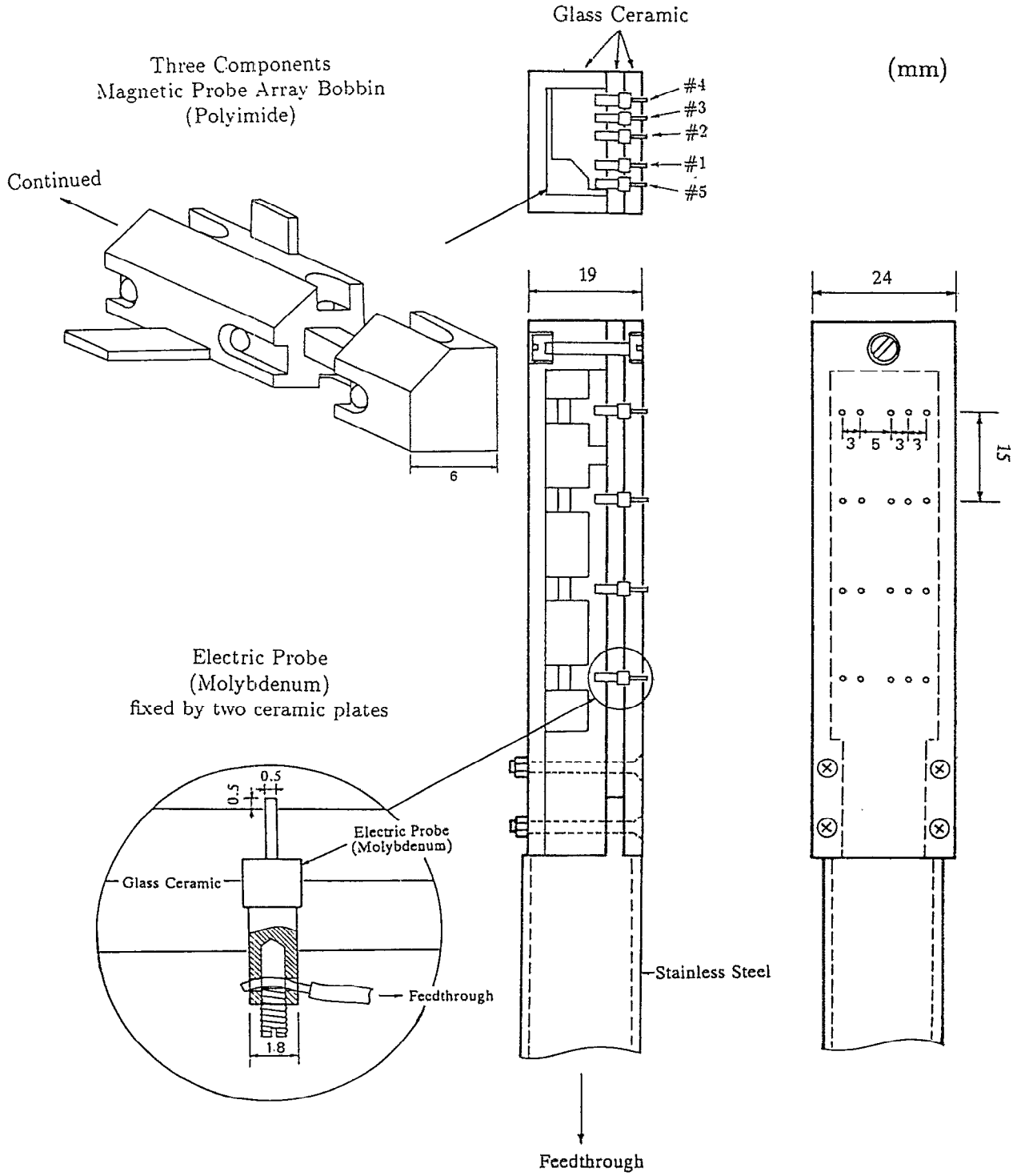


FIG. 8. Structure of a triple-probe and magnetic-probe array.

the magnetic fields at the same positions corresponding to the triple probes, simultaneously. This probe bobbin, as shown in Fig. 8, is made of polyimide which has a lower outgas level in the vacuum, and was designed as to avoid the crosstalk between the three components as possible. The calibrations of the magnetic probes are performed using a Helmholtz coil driven by a power amplifier of 1 kW or using the vacuum toroidal fields. Absolute accuracies of the calibrations agree with each other by these two methods within 2%. The relative accuracies between the different channels are carefully calibrated within 0.5%. The leads from the magnetic probes are brought out as a tightly twisted pair in a 25-pair shielded cable, and transmitted to the active integrators to reduce a common mode noise.

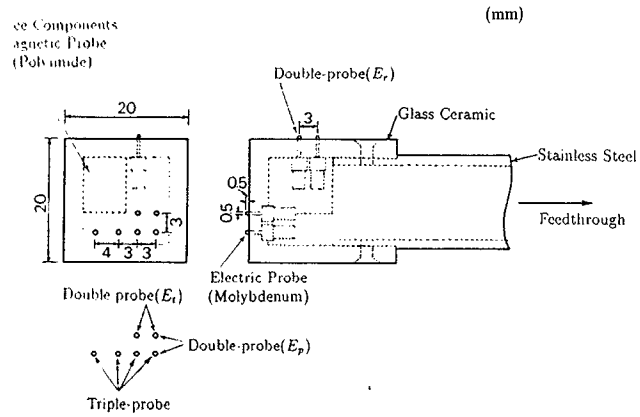


FIG. 9. Schematic view of the complex probe.

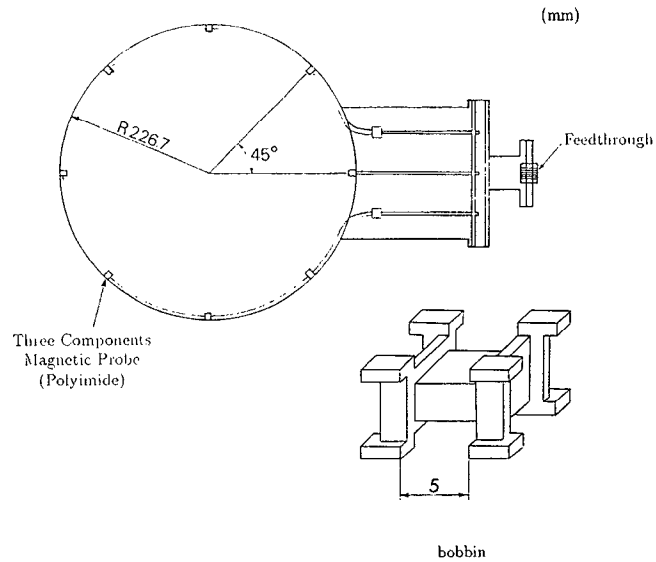


FIG. 10. Poloidal array of magnetic probes, consisting of two square cross-section pipes and eight three-components magnetic probes wound on the specially designed bobbins.

## B. Complex probe

A complex probe was designed for measuring the mean and fluctuation parts of various plasma parameters, including density $n$, electron temperature $T_e$, three components of magnetic field $B_t$, $B_p$, and $B_r$, three components of electric field $E_t$, $E_p$, and $E_r$, at the almost same point in space (within 10 mm$\times$10 mm$\times$15 mm). The schematic view of the complex probe is shown in Fig. 9. If only the fluctuations of $n$, $T_e$, $E_t$, and $E_p$ are concerned, the spread in space then becomes smaller, within 10 mm$\times$4 mm$\times$1 mm. The correlations between fluctuations of these parameters can be determined in one shot.

The complex probe consists of a triple-probe, three-components magnetic probe, and three pairs of double probes. The triple probe consists of four Molybdenum tips, having the same structure composition as described in the previous section. The magnetic probe is the same one as that used in the poloidal magnetic probe array (see Fig. 10). The electric fields are measured by three pairs of double probes. The leads from the double probe are carefully brought out as a tightly twisted pair in a four-pair shielded cable, and are transmitted to the isolation amplifier (Fig. 13) to reduce a common mode noise.

## C. Poloidal and toroidal magnetic-probe arrays

In order to observe the high-frequency components of the magnetic fluctuations, a poloidal array of magnetic field pick-up coils with protective covers of 0.7-mm-thick stainless steel is installed at P-3 port segment inside the vacuum vessel (Fig. 14). Two pipes with a square cross section leads the coil signal wires to the feedthrough flange and protects them from the plasma, as shown in Fig. 10. The array covers all poloidal angle equally at eight poloidal positions with a 45° separation. At each position three components of fields $B_t$, $B_p$, and $B_r$ can be measured by the specially designed probe bobbin (Fig. 10) simultaneously, with a frequency response up to 40 kHz. With the use of this poloidal array, the time-varying equilibrium quantities (such as the plasma position and Shafranov's parameter $\Lambda$) can be determined based on a simple fitting method.[32]

A toroidal array of magnetic field pick-up coils with protective pipes of 1.0-mm-thick stainless steel is installed between the bottom of P-1 and P-3 port segment inside the vacuum vessel (Fig. 14). Two pipes of 1-cm-diam leads the coil signal wires to the feedthrough parts at the P-1, P-2, and P-3 bottom ports. The array covers 40° of the toroidal angle with eight equally spaced positions, as shown in Fig. 11. At each position three components of fields $B_t$, $B_p$, and $B_r$ can be measured simultaneously, with a frequency response up to $\sim$30 kHz.

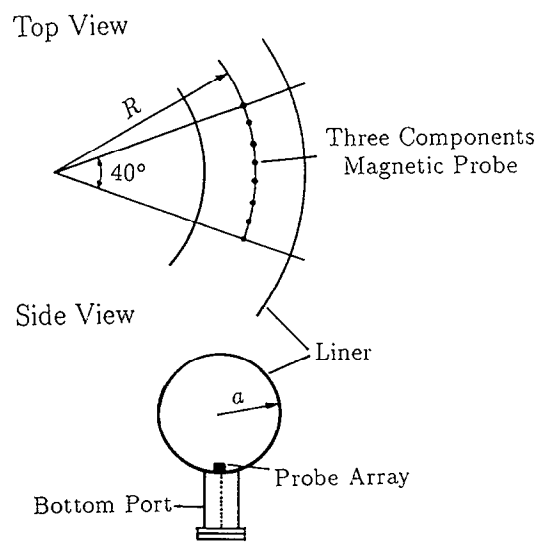


FIG. 11. Toroidal magnetic probe array which covers 40° of toroidal angle with eight equally spaced positions.

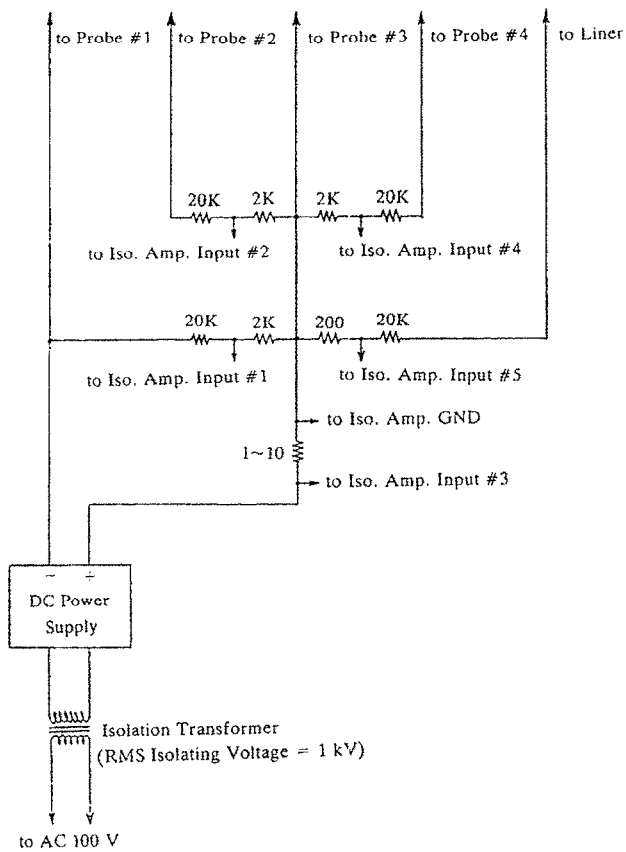


FIG. 12. A triple-probe drive circuit. Here, Probe No. 1~4 correspond P1~4 in Fig. 4.

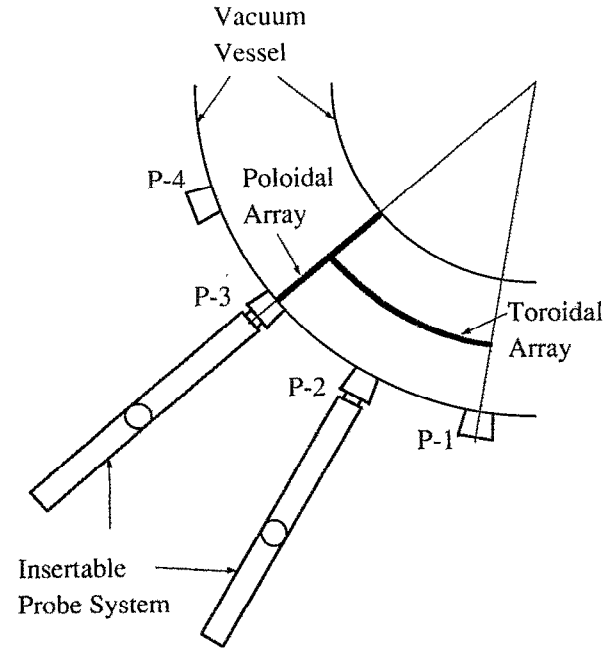


FIG. 14. Top view of arrangement of probe measurements in REPUTE-1.

## D. Probe drive circuit and data-acquisition electronics

The probe driver consists of five triple-probe drive circuits, five single-probe drive circuits, and three double-probe drive circuits. A triple-probe drive circuit is shown in Fig. 12, where a dc power supply is isolated from the earth. The voltages between the probes or liner are divided into 1/10 or 1/100 in order to match the input levels of the isolation amplifiers. The probe currents are monitored by series resistors of 1~10 Ω.

The 36 isolation amplifiers in total were made, with a special design considering the response frequency. The detailed electronic circuit is shown in Fig. 13. Photocouplers (TLP551O, TOSHIBA) used for electric isolation have a response frequency up to 2 MHz. When driver circuits for photocoupler and an operational amplifier LF357N are combined, the total circuit still has a response frequency up to 250 kHz.

Each triple probe and single probe use five and two isolation amplifiers, respectively. The remaining eight isolation amplifiers are used for measuring the fluctuations of electric fields and for another triple probe in the complex probe.

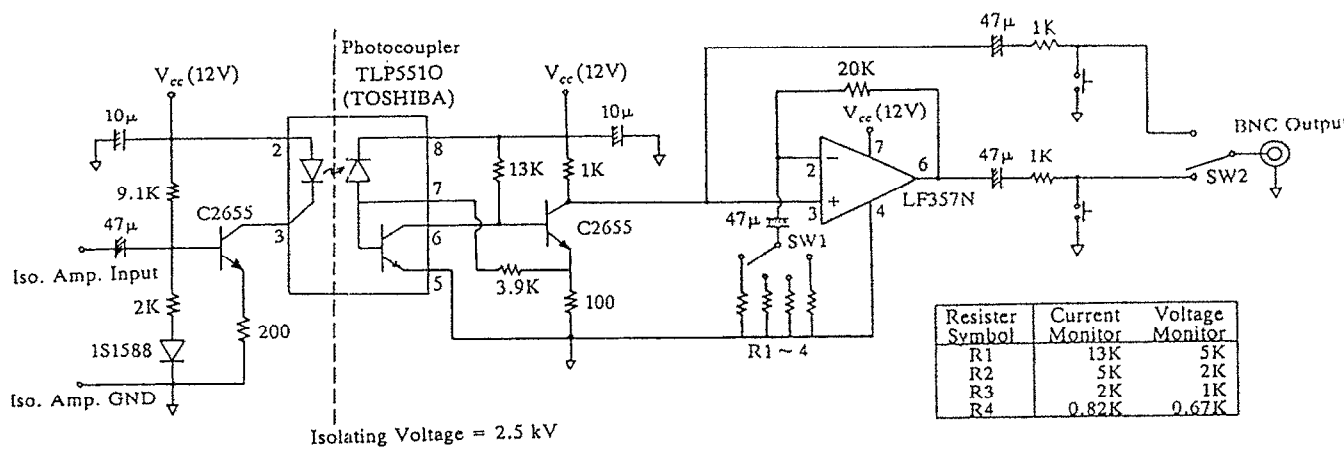


| Resister Symbol | Current Monitor | Voltage Monitor |
|---|---|---|
| R1 | 13K | 5K |
| R2 | 5K | 2K |
| R3 | 2K | 1K |
| R4 | 0.82K | 0.67K |

FIG. 13. Circuit of an isolation amplifier with a response frequency up to 250 kHz.

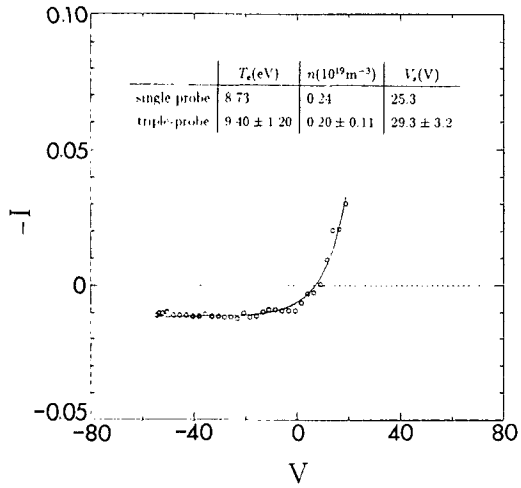


FIG. 15. An example of $I$-$V$ curve fitting for the single-probe measurements at $r=19$ cm. The time-averaged results from the simultaneous triple-probe measurement are also shown for the comparison.

## IV. SOME EXAMPLES OF MEASUREMENT

In this section, we present some experimental examples obtained in the REPUTE-1 RFP plasma using probes described above. Figure 14 shows a top view of arrangement of probe measurements in REPUTE-1 which has a major radius of 82 cm and a minor radius of 22 cm. Two insertable probe systems[33] are located on the side ports of P-3 and P-2. A differential pumping system is used for easy change of probes. The triple-probe and magnetic-probe array was installed in the insertable probe system on the P-3 port, and the tip of probe array can be inserted radially into $r=6$ cm from the plasma edge. The complex probe was installed in the insertable probe system on the P-2 port which has 20° apart in the toroidal angle from the P-3 port. The probe can be inserted into the plasma from the edge to $r=10$ cm. The poloidal and toroidal magnetic-probe arrays were installed at the P-3 port and the bottom between the P-1 and P-3 port, respectively.

Usually, the probe measurements are performed in the low current discharges in which the plasma current $I_p$ is less than 120 kA, in order to avoid high heat load to the probe. At the current flat-top phase of a typical discharge, the plasma current, loop voltage, the reversal ratio $F$, the pinch parameter $\Theta$, and the chord-averaged density are $I_p \sim 110$ kA, $V_l \sim 220$ V, $F \sim -0.4$, $\Theta \sim 2.0$, and $\bar{n}_e \sim 0.44 \times 10^{20}\,\mathrm{m}^{-3}$, respectively. Central ion temperature $T_i(0) \sim 100$ eV measured from the Doppler width of $OV$ line, is about twice of $T_e(0) \sim 50$ eV, measured by a Thomson scattering system. Hereafter, in order to obtain the density $n$ in Eq. (2), the ion temperature $T_i$ is assumed to be twice of $T_e$, although there is no information on $T_i$ except at the center.

As a cross check for the triple-probe measurements,

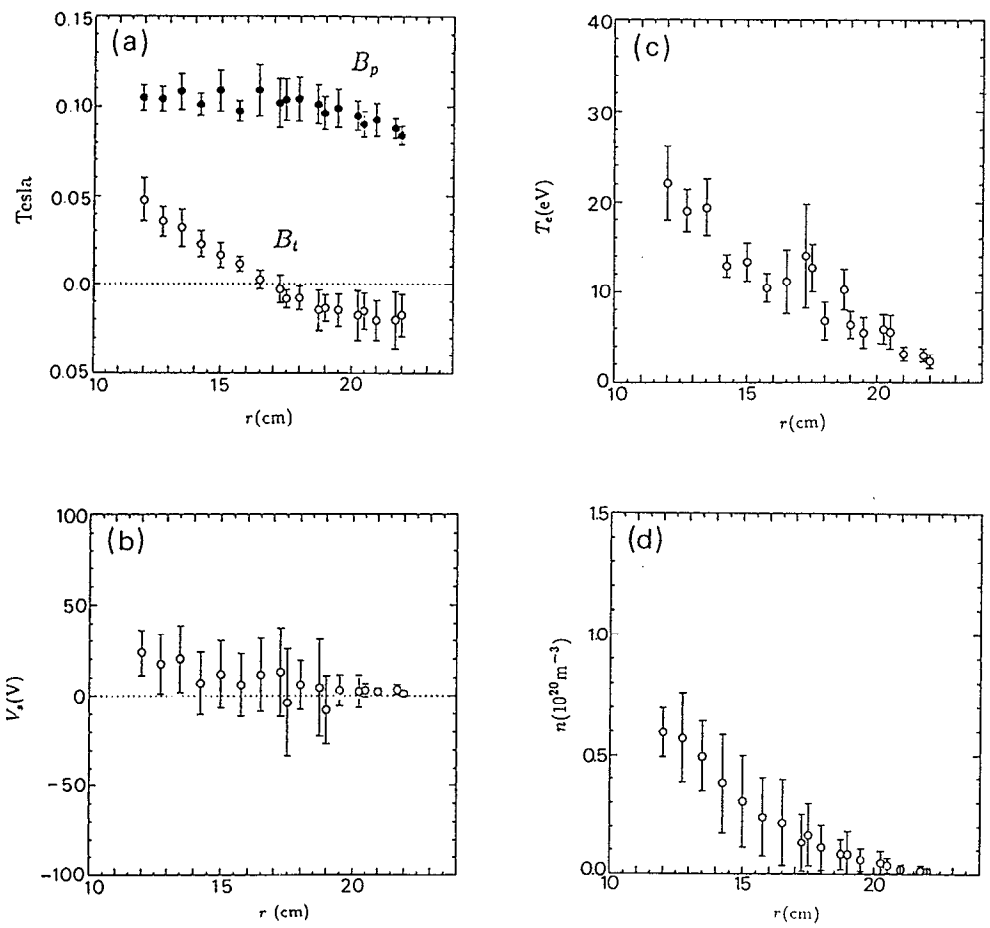


FIG. 16. Radial profiles of the toroidal and poloidal field (a), electron density (b), electron temperature (c), and space potential (d). The error bars represent root mean square errors shot by shot.

the single-probe in the same channel in the triple-probe and magnetic-probe array (Sec. III A) was drived by a 5 kHz ac amplifier with a range of $\pm 60$ V to obtain a current-voltage characteristic($I$-$V$ curve) of the Langmuir probe. After removing the fast fluctuations, the $I$-$V$ curves were well fitted to those predicted by Eq. (3), regurding $T_e$, $n$, and $V_s$ as the fitting parameters. An example measured at $r=19$ cm is shown in Fig. 15. The fitting results agree well with the time averaged those obtained from the simultaneous triple-probe measurement. In order to examine the effects due to the fast electrons experimentally, we inserted a triple-probe with an obstacle nearby into the plasma. Comparing the results obtained in the three cases, i.e., with/without the obstacle upstream/downstream the field line, we found no more observable differences between them than the shot-by-shot variation, therefore, we do not expect a significant perturbation to our triple-probe measurements.

Figure 16 shows edge profiles of the toroidal field $B_t$, poloidal field $B_p$, electron density $n$, electron temperature $T_e$, and space potential $\phi_s(\equiv V_s)$ in $0.5a \lesssim r \leqslant a$ region, obtained by the triple-probe and magnetic-probe array. The error bars indicate the shot-by-shot variation. The poloidal field $B_p$ decreases slightly with $r$, and toroidal field $B_t$ reverses its direction at $r\sim 17$ cm. As the radius decreases, $n$, $T_e$, and $\phi_s$ increase to $\sim 6.0\times 10^{19}$ m$^{-3}$, $\sim 22$ eV, and $\sim +25$ V at $r\sim a/2$, respectively.

As another example, spectra of the magnetic fluctuations measured by the poloidal and toroidal magnetic arrays are presented. By performing Fourier decomposition both in time and space (e.g., the poloidal angle $\theta$) on the two-dimensional signals $x(\theta_i,t_j)$ where $0\leqslant i\leqslant I$ and $0\leqslant j\leqslant J$:

$$X(m,\omega)=\frac{1}{IJ}\sum_{i,j} x(\theta_i,t_j)\exp[i(m\theta_i-\omega t_j)], \qquad (40)$$

where mode number $m$ can be taken as a positive or negative numbers. For the eight channels of the poloidal array, the poloidal mode number can be determined from $-3$ to 3. Therefore, the $m$ power spectrum is obtained by

$$P(m)=\sum_{\omega} P(m,\omega), \qquad (41)$$

where $P(m,\omega)=X^*(m,\omega)X(m,\omega)$. Similar procedure can be done with signals from the toroidal array. The toroidal mode number $n$ in the range from $-31$ to 31 with a resolution of $\Delta n=9$ can be determined. Figure 17 shows the measured spectra of the poloidal (toroidal) mode number $m(n)$ for the radial field fluctuations $\tilde{B}_r$, where the spectra are normalized by the total fluctuation power. The error bars indicate the variation due to shot by shot. It can be seen that the most fluctuation power concentrates in the modes of $-1\leqslant m\leqslant 1$ and $-13\leqslant n\leqslant 13$, especially $m=0$ and $-4\leqslant n\leqslant 13$.

The further detailed results, e.g., the edge profiles of fluctuation levels, discussions on relations between electrostatic/magnetic fluctuations and the energy transport, etc., will be published elsewhere.[27]

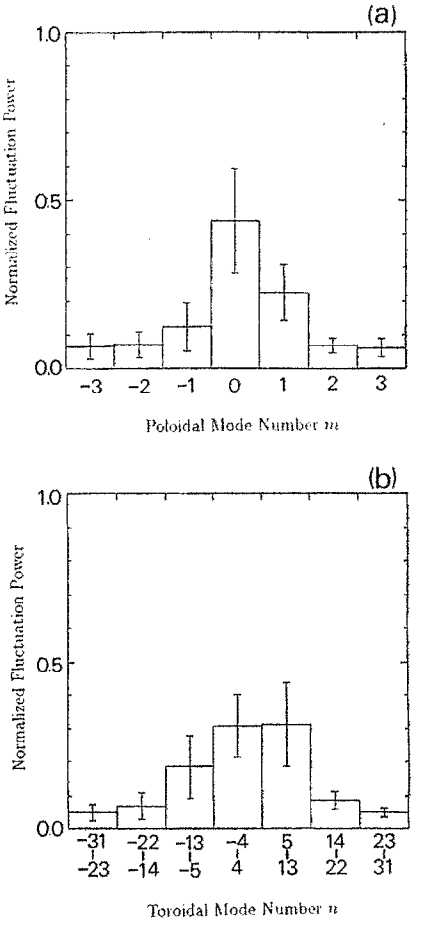


FIG. 17. Normalized power spectrum of poloidal mode number $m$ (a) and toroidal mode number $n$ (b) for radial field fluctuations.

## ACKNOWLEDGMENTS

The authors wish to thank Y. Shimazu, A. Ejiri, A. Shirai, S. Ohdachi, and K. Mayanagi for their help in the probe installations. Dr. K. Itami, who designed the toroidal magnetic-probe array, is also acknowledged.

[1] P. C. Stangeby, Nucl. Fusion **30**, 1225(1990).
[2] P. C. Liewer, Nucl. Fusion **25**, 543(1985).
[3] F. F. Chen, in *Plasma Diagnostic Techniques*, edited by R. H. Huddletone and S. L. Leonard (Academic, New York, 1965), p. 113.
[4] D. M. Manos, J. Vac. Sci. Technol. A **3**, 1059(1985).
[5] P. C. Stangeby, in *Plasma Diagnostics*, edited by O. Auciello and D. Flamm (Academic, Boston, 1988), Vol. 1, p. 157.
[6] I. H. Hutchinson, *Principles of Plasma Diagnostics* (Cambridge University, Cambridge, 1987).
[7] N. Asakura *et al.*, in *Proceedings of 11th International Conference on Plasma Physics and Controlled Nuclear Fusion Research, Kyoto, Japan, 1986*, edited by J. W. Weiland and M. Demir (IAEA, Vienna, 1987), Vol. 2, p. 433.
[8] L. Tonks and I. Langmuir, Phys. Rev. **34**, 876(1929).
[9] D. Bohm, E. H. S. Burshop, and H. S. W. Massey, in *The Characteristics of Electrical Discharges in Magnetic Fields*, edited by A. Guthrie and R. K. Wakerling (McGraw-Hill, New York, 1949).
[10] J. Laframboise, in *Rarefied Gas Dynamics*, edited by J. H. de Leeum (Academic, New York, 1966), Vol. 2, p. 22.
[11] P. C. Stangeby, Phys. Fluids **27**, 682(1984).
[12] P. C. Stangeby, J. Phys. D **15**, 1007(1982).
[13] P. C. Stangeby, Phys. Fluids **27**, 2699(1984).

[14] P. C. Stangeby, Phys. Fluids **30**, 3262(1987).
[15] I. H. Hutchinson, Phys. Fluids **30**, 3777(1987).
[16] I. H. Hutchinson, Phys. Rev. A **37**, 4358(1988).
[17] R. C. Bissell, P. C. Johnson, and P. C. Stangeby, Phys. Fluids B **1**, 1133(1989).
[18] J. T. Scheuer and G. A. Emmert, Phys. Fluids B **2**, 445(1990).
[19] G. A. Emmert, R. M. Wieland, A. T. Mense, and J. N. Davidson, Phys. Fluids **23**, 803(1980).
[20] R. C. Bissell, Phys. Fluids **30**, 2264(1987).
[21] J. T. Scheuer and G. A. Emmert, Phys. Fluids **31**, 3645(1988).
[22] K-S. Chung and I. H. Hutchinson, Phys. Fluids **28**, 4721(1988).
[23] K. Sato, F. Miyawaki, and W. Fukui, Phys. Fluids B **1**, 725(1989).
[24] E. R. Harrison and W. B. Thompson, Proc. Phys. Soc. London **74**, 145(1959).
[25] S-L. Chen and T. Sekiguchi, J. Appl. Phys. **36**, 2363(1965).
[26] H. Ji, S. Matsuzuka, A. Fujisawa, S. Shinohara, K. Yamagishi, H. Toyama, and K. Miyamoto, in *Proceedings of the 15th European Conference on Controlled Fusion and Plasma Physics, Dubrovnik, 1988*, edited by S. Pesic and J. Jacquinot (European Physical Society, Dubrovnik, 1988), Part 2, p. 545.
[27] H. Ji, Ph.D. Thesis, University of Tokyo ,1990; H. Ji, H. Toyama, K. Miyamoto, S. Shinohara, and A. Fujisawa, Phys. Rev. Lett. **67**, 62 (1991).
[28] J. C. Ingraham, R. F. Ellis, J. N. Downing, C. P. Munson, P. G. Weber, and G. A. Wurden, Phys. Fluids B **2**, 143 (1991).
[29] S. J. Levinson, J. M. Beall, E. J. Powers, and R. D. Bengtson, Nucl. Fusion **24**, 527 (1984).
[30] Ch. P. Ritz, R. D. Bengtson, S. J. Levinson, and E. J. Powers, Phys. Fluids **27**, 2956 (1984).
[31] G. Miller, J. C. Ingraham, C. P. Munson, K. F. Schoenberg, and P. G. Weber, in *Proceedings of the 17th European Conference on Controlled Fusion and Plasma Physics, Amsterdam, 1990,* edited by G. Brifford, A. Nigsen-Vis, and F. C. Schuller (European Physical Society, Amsterdam, 1990), Part 2, p. 581.
[32] H. Ji, H. Toyama, S. Shinohara, A. Fujisawa, and K. Miyamoto, Plasma Phys. Contr. Fusion **32**, 79 (1990).
[33] Y. Ueda, N. Asakura, S. Matsuzuka, K. Yamagishi, S. Shinohara, Y. Nagayama, H. Toyama, and K. Miyamoto, Nucl. Fusion **27**, 1453 (1987).